Sensors & Diagnostics

Accepted Manuscript

This article can be cited before page numbers have been issued, to do this please use: D. Mohanapriya and T. Kathavarayan, *Sens. Diagn.*, 2025, DOI: 10.1039/D5SD00114E.

ROYAL SOCIETY OF CHEMISTRY

rsc.li/sensors

View Article Online
DOI: 10.1039/D5SD00114E

ARTICLE

Surface modified titanium carbide MXene as an effective platform for immobilization of toluidine blue and H_2O_2 biomarker detection in biological samples

Devarasu Mohanapriya and Kathavarayan Thenmozhi*

Development of reliable and cost-effective electrochemical sensors towards hydrogen peroxide (H_2O_2) monitoring is crucial in biomedical diagnostics, especially towards early disease diagnosis. Herein, we have prudently synthesized an acid-functionalized COOH-$Ti_3C_2T_x$ MXene, to which the toluidine blue (TB) redox mediator has been covalently immobilized and employed towards the distinctive determination of H_2O_2. The synthesized COOH-$Ti_3C_2T_x$ was coated over glassy carbon electrode (GCE), followed by the covalent immobilization of the electroactive TB dye through N-(3-dimethylaminopropyl)-N′-ethylcarbodiimide hydrochloride (EDC)/ N-hydroxysuccinimide (NHS) coupling reaction. This in turn results in the firm anchoring of the TB dye by establishing a stable amide linkage between -COOH group of COOH-$Ti_3C_2T_x$ and the free -NH_2 group of TB. Thus obtained TB/COOH-$Ti_3C_2T_x$-GCE sensor demonstrated an excellent electrocatalytic response for H_2O_2 determination over a broad linear range of 5 μM to 100 μM and 100 μM to 1.1 mM with high sensitivity of 0.61 μA μM^{-1} cm^{-2} and a low detection limit of 1.5 μM. Notably, the proposed fabricated electrode demonstrated exceptional stability and reproducibility as well as high selectivity and sensitivity for the detection of H_2O_2. Furthermore, the developed sensor has shown very good recovery towards the detection of H_2O_2 in milk and serum samples. The attained analytical performance is attributed to the improved electrical wiring between the TB mediator and conductive MXene platform.

Received 00th January 20xx,
Accepted 00th January 20xx

DOI: 10.1039/x0xx00000x

1. Introduction

Hydrogen peroxide (H_2O_2) is one of the most important by-products of metabolic processes in the human body and plays a major role in various physiological functions. However, excessive production of H_2O_2 can have detrimental effect in brain and tissues, which might lead to several life-threatening issues such as cardiovascular disease, Alzheimer's disease and cancer.[1–4] Accordingly, H_2O_2 is regarded as a distinctive biomarker towards early diagnosis of various diseases including Alzheimer's, asthma, chronic obstructive pulmonary, Parkinson's, cancer and periodontitis, and thus, a simple, cost-effective, sensitive and accurate measurement of H_2O_2 becomes necessitous. H_2O_2 has been detected thus far using various quantification techniques like spectrophotometry, fluorescence, titrimetry, resonance light scattering and chemiluminescence. Unfortunately, many of these techniques are costly, time-consuming and complicated, limiting their application in monitoring H_2O_2 in real-time samples.[5–8] Among the several methods, electrochemical determination of H_2O_2 is strongly recommended over its counterparts because of its ease of sample preparation, affordability, sensitivity and selectivity.[9,10] In recent years, the electrocatalytic detection of H_2O_2 has been extensively researched using numerous modified electrodes to address its oxidation or reduction. Amongst these, enzymatic electrochemical biosensors encompass the benefit of excellent sensitivity and selectivity.[11–13] In contrast, their application is restricted owing to the expensive nature of enzymes, laborious immobilization processes, poor repeatability and environmental instability.[14]

Non-enzymatic electrochemical sensors have been utilized as an efficient alternate for biosensors, since it not only enhances the durability of the sensor, but also enables the detection of H_2O_2 at lower potentials.[15] These non-enzymatic sensors can be prepared through electrochemical pre-treatment, polymerization, mediator adsorption or self-assembly and covalent immobilization of mediators over a conductive substrate.[11] Mediators often include organic salts, metal complexes, quinones, catechols and redox dyes. However, electrodes fabricated by simple adsorption process would quickly lose their electrocatalytic activity due to lack of proper immobilization.[16,17] The technique utilized to immobilize the mediators is a crucial step in the fabrication of modified electrodes and has a significant impact on the sensitivity and stability of the sensor. Thus, covalent immobilization of mediators is the most appropriate technique to prepare highly stable leak-free sensors.[18] Organic dye molecules like Azure A, methylene blue, methylene green and toluidine blue (TB) have been employed as a mediator to investigate the electrocatalytic reduction of H_2O_2 owing to their well-defined redox behaviour, which helps to facilitate the electron transfer during the electrochemical process.[19,20] TB has been chosen as a mediator for this study because of its well-defined redox behaviour at lesser potential, good electrochemical stability and

Department of Chemistry, School of Advanced Sciences, Vellore Institute of Technology (VIT), Vellore-632014, India.
Electronic Supplementary Information (ESI) available: Materials, Instrumentation, FESEM image and elemental analysis of Ti_3AlC_2 and $Ti_3C_2T_x$ NSs, XPS survey spectra of $Ti_3C_2T_x$ NSs and COOH-$Ti_3C_2T_x$ NSs, Core level spectrum of Ti 2p in $Ti_3C_2T_x$ NSs and COOH-$Ti_3C_2T_x$ NSs, Effect of scan rate and corresponding calibration plot, real-time analysis.

potential to boost the electron transfer between the electrode and the electrolyte interface.[21] The major drawback of using TB or other similar dyes-based electrochemical sensors over an extended period is that they gradually disintegrate from the electrode surface due to their water solubility, resulting in fouling of electrode along with subsequent loss in sensitivity and durability. This limitation could be resolved via the covalent anchoring of these redox dyes/mediators on a stable substrate.[22] The development of sensors for ambient or in-vivo analysis requires such careful consideration of this immobilization aspect.

The choice of an appropriate substrate material to immobilize the redox mediator is crucial in developing a successful sensor. Novel 2D single layer transition metal carbide and nitride MXene nanosheets (NSs) have been rising as a potential host material for electrochemical sensors compared to existing 2D materials like graphene oxide (GO), graphitic carbon nitride (g-C_3N_4) and multi walled carbon nanotube (MWCNT).[23–27] Precisely, in the family of 2D MXenes, titanium carbide MXene ($Ti_3C_2T_x$) has been well explored for various applications by virtue of its intriguing properties such as excellent conductivity, high surface area, outstanding electrochemical stability and good hydrophilicity.[28,29] Since terminal groups account for most of the characteristics of $Ti_3C_2T_x$, prudently designing these $Ti_3C_2T_x$ MXene with functional groups such as -COOH and -NH_2, could advantageously aid in the covalent immobilization of dye molecule.[30]

To the best of our knowledge, no efforts have been made so far to fabricate a disintegration-free electrochemical sensor towards the detection of H_2O_2 biomarker using TB and acid functionalized MXene (COOH-$Ti_3C_2T_x$). This prompted us to fabricate an electrochemical sensor towards H_2O_2 detection through covalent immobilization of TB over COOH-$Ti_3C_2T_x$ MXene. In this regard, the redox active TB was coupled to the COOH-$Ti_3C_2T_x$ NSs via N-(3-dimethylaminopropyl)-N′-ethylcarbodiimide hydrochloride (EDC)/ N-hydroxysuccinimide (NHS) coupling reaction, which led to the stable anchoring of TB. Additionally, the constructed electrochemical sensor demonstrated a broad detection range and good sensitivity towards H_2O_2 detection. The synthesized surface functionalized $Ti_3C_2T_x$ proved to be a great anchoring site for the mediator immobilization and thus the constructed sensor was highly stable and reproducible. This is of great significance as lack of effective immobilization would result in diminished current response because of the dissolution of the water soluble TB in aqueous electrolyte. Furthermore, the fabricated electrochemical sensor demonstrated remarkable electrochemical performance for the determination of H_2O_2 in milk and serum samples paving an effective approach towards early disease diagnosis.

2. Experimental Section

All chemicals and instrumentation details are given in the electronic supplementary information (ESI).

2.1. Synthesis of $Ti_3C_2T_x$ NSs

In this study, we synthesized $Ti_3C_2T_x$ NSs using a safer and more environment friendly in-situ HF wet acid etching method that we had reported previously.[31,32] Typically, as illustrated in Fig. 1a, 1 g of Ti_3AlC_2 MAX phase powder was slowly added to an etching solution which consisted of 1 g of lithium fluoride (LiF) and hydrochloric acid (9 M HCl). The mixture was kept for 24 h stirring at room temperature (RT) to remove the Al layer from Ti_3AlC_2. Thereafter, the resulting mixture was washed with deionized water by centrifugation until the pH of the solution reached 6. Following that, the obtained solution was subjected to ultrasonication for 1 h at N_2 atmosphere to get homogenously dispersed $Ti_3C_2T_x$ NSs. Later, the sample was freeze dried at -60 ℃ and stored in vacuum desiccator for further characterization.

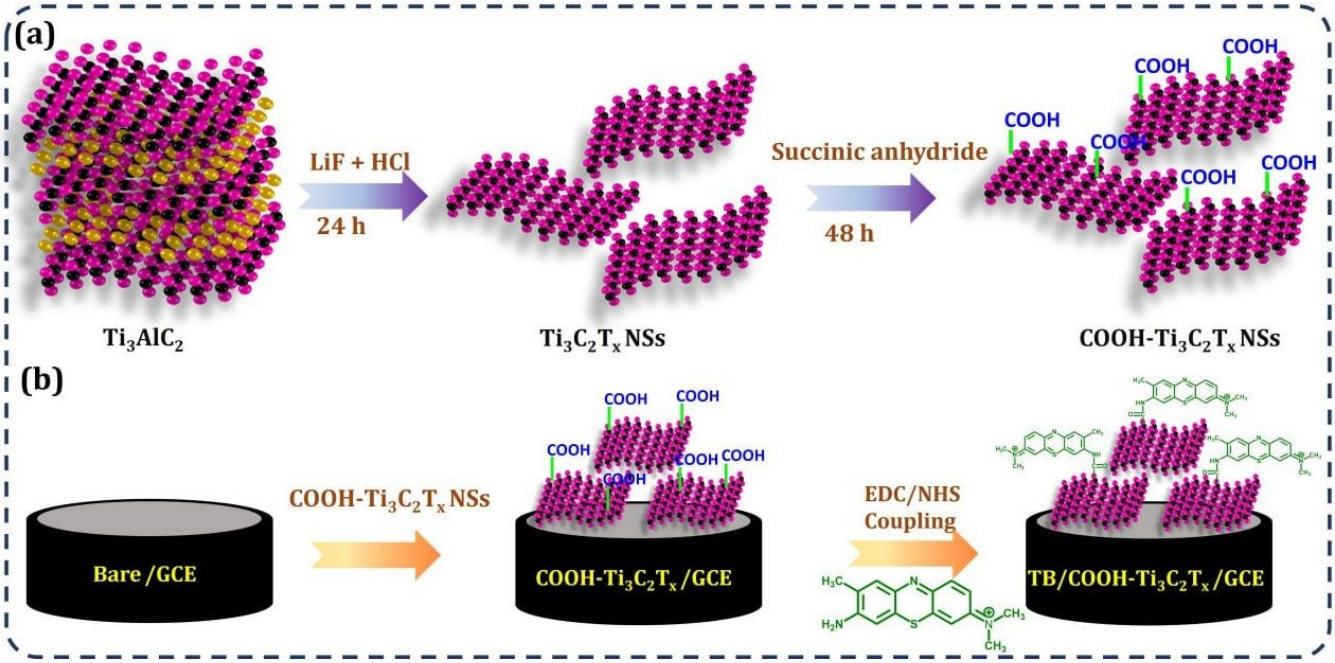

Fig. 1 (a) Schematic representation for the synthesis of $Ti_3C_2T_x$ NSs and COOH-$Ti_3C_2T_x$ NSs (b) Stepwise fabrication of TB/COOH-$Ti_3C_2T_x$/GCE.

DOI: 10.1039/D5SD00114E

2.2. Synthesis of COOH-$Ti_3C_2T_x$ NSs

After the successful preparation of $Ti_3C_2T_x$ NSs comprising of terminal -OH functional groups, we further intended to functionalize these $Ti_3C_2T_x$ NSs with -COOH functional groups, which in turn will be beneficial for the covalent immobilization of redox dye molecules. The readily reactive -OH groups were subjected to ring-opening followed by an esterification reaction with succinic anhydride, which enabled the introduction of carboxylic acid functional groups into the $Ti_3C_2T_x$ NSs surface to produce acid functionalized MXene (COOH-$Ti_3C_2T_x$) NSs (Fig. 1a). Precisely, 0.5 g of $Ti_3C_2T_x$ NSs was dispersed in 25 mL of ethanol using ultrasonication. Meanwhile, 5 g of succinic anhydride was added to 25 mL of ethanol and transferred to the $Ti_3C_2T_x$ NSs-ethanol mixture and the reaction mixture was kept at constant stirring at 300 rpm for 48 h.[33] The obtained precipitate was rinsed thoroughly with DI water and centrifuged at 3000 rpm until all the remaining residual succinic anhydride was removed. Afterwards, the centrifugate was vacuum dried for 12 h at 25 ℃ to obtain COOH-$Ti_3C_2T_x$ NSs.

2.3. Sensor fabrication through covalent immobilization of TB on COOH-$Ti_3C_2T_x$ platform

The TB modified electrode was prepared by the following steps. Initially, the bare glassy carbon electrode (GCE) was polished thoroughly using alumina powder and ultrasonicated using an ethanol and water mixture for 5 min to achieve a mirror clean electrode surface. Thereafter, 10 µL of COOH-$Ti_3C_2T_x$ NSs (2 mg in 200 µL of ethanol) was drop-casted on top of the polished electrode. After drying, the carboxyl groups present on the $Ti_3C_2T_x$ NSs were further activated using 5 µL of 2 mM EDC in 0.1 M phosphate buffer solution (PBS) followed by 5 µL of 5 mM NHS in 0.1 M PBS for 60 min each. Thereafter, the modified electrode was dipped into TB solution (2 mg in 0.5 mL ethanol) for 1 h to facilitate the covalent immobilization of the redox mediator. Further, the fabricated TB/COOH-$Ti_3C_2T_x$-GCE was washed gently with PBS to remove loosely adsorbed TB. Then, 5 µL of 1% nafion was coated over the constructed TB/COOH-$Ti_3C_2T_x$-GCE to enhance the stability.

3. Results and discussion

3.1. Characterization of $Ti_3C_2T_x$ and COOH-$Ti_3C_2T_x$ NSs

The morphology and elemental composition of the Ti_3AlC_2, $Ti_3C_2T_x$ NSs and COOH-$Ti_3C_2T_x$ NSs were probed using field emission scanning electron microscopy (FESEM) and scanning electron microscopy (SEM) with elemental mapping. The MAX phase precursor Ti_3AlC_2 demonstrated the closed layered structure comprising Al and is displayed in Fig. S1. On the other hand, the synthesized $Ti_3C_2T_x$ NSs reveal well separated NS like morphology which indicates the

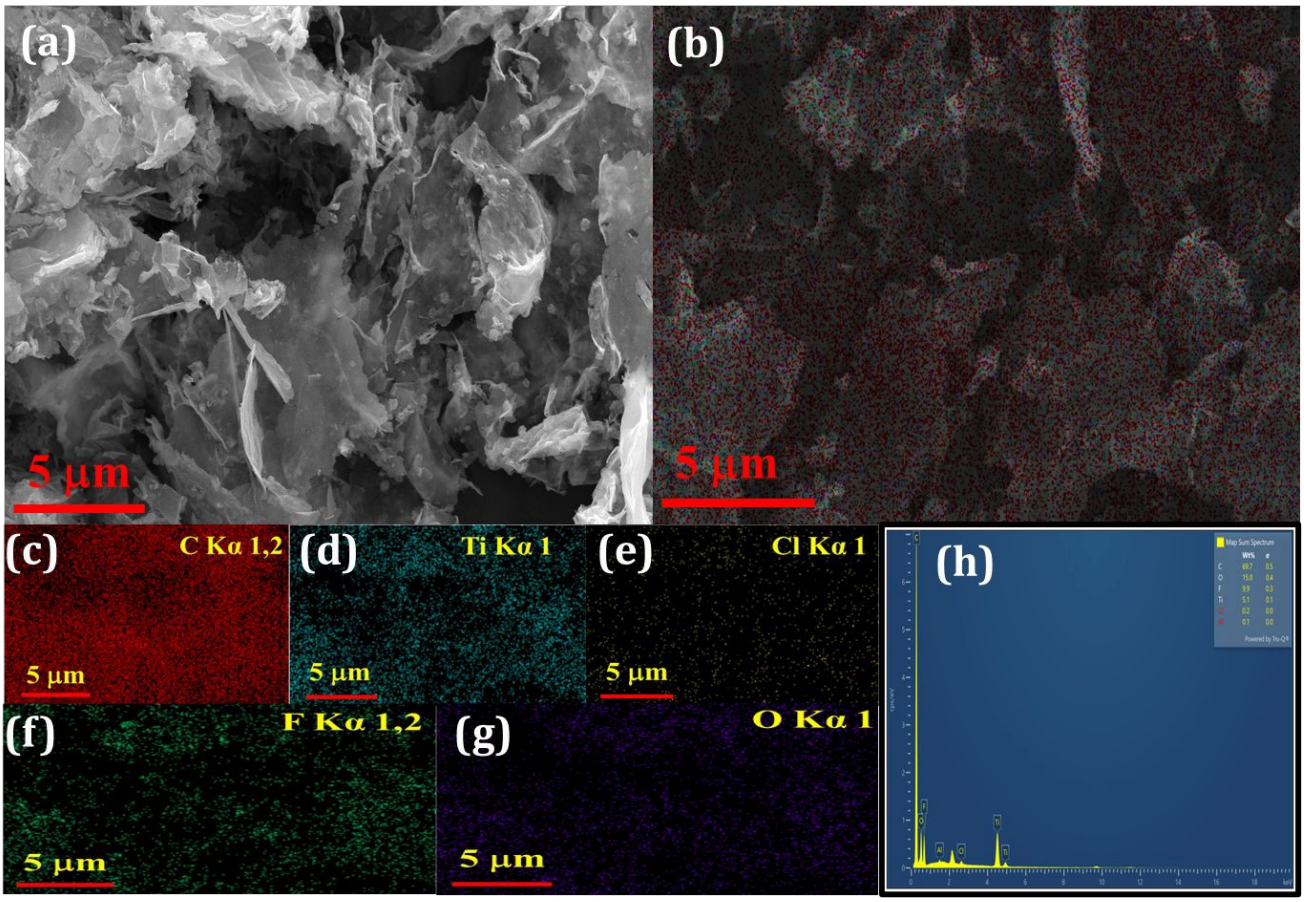

Fig. 2 (a) FESEM images (b-g) Elemental mapping and (h) EDX analysis of COOH-$Ti_3C_2T_x$ NSs.

View Article Online
DOI: 10.1039/D5SD00114E

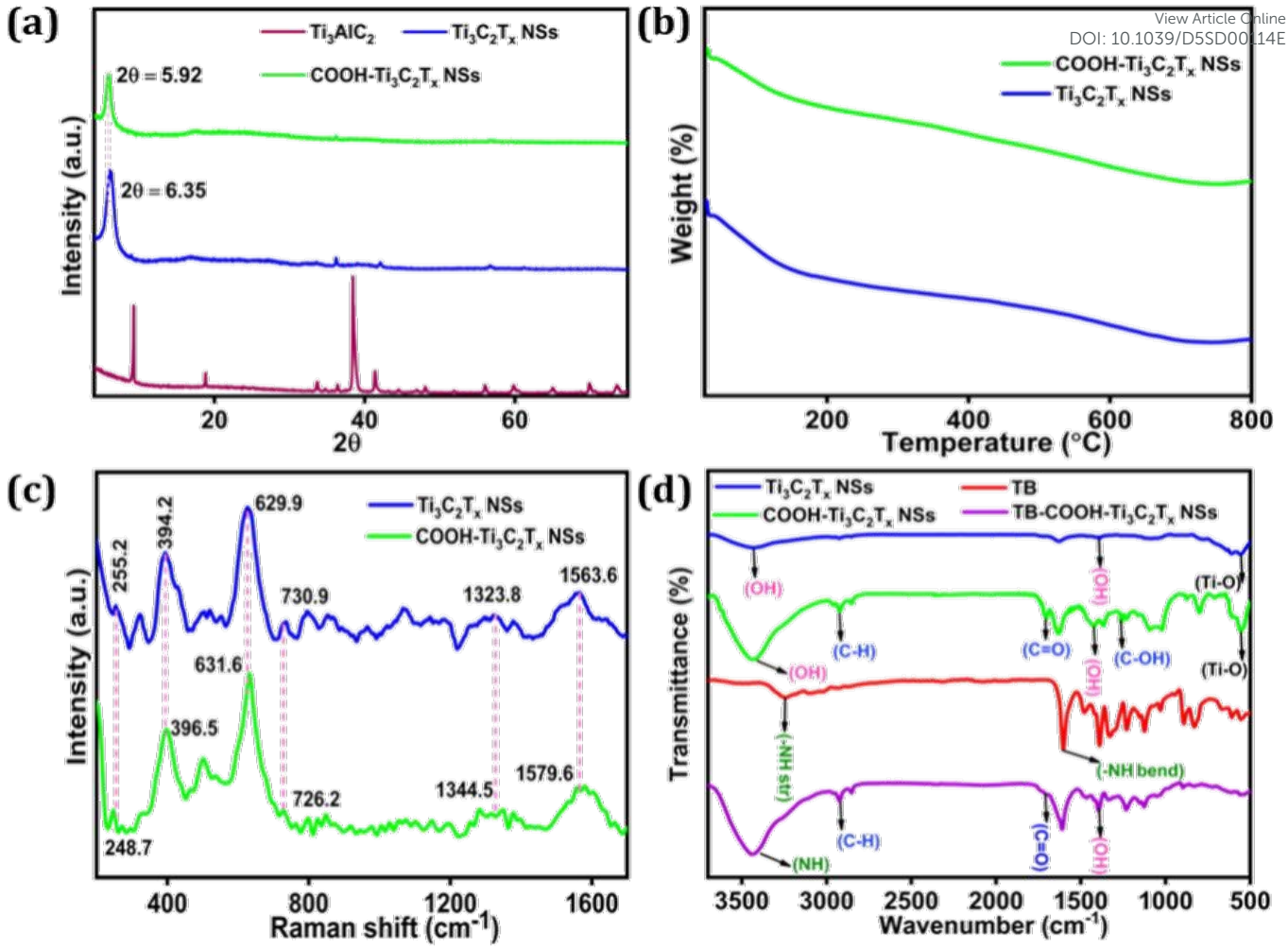

Fig. 3 (a) XRD patterns of Ti_3AlC_2, $Ti_3C_2T_x$ NSs and COOH-$Ti_3C_2T_x$ NSs (b) TGA curves of $Ti_3C_2T_x$ NSs and COOH-$Ti_3C_2T_x$ NSs (c) Raman spectra of $Ti_3C_2T_x$ NSs and COOH-$Ti_3C_2T_x$ NSs (d) FTIR spectra of $Ti_3C_2T_x$ NSs, COOH-$Ti_3C_2T_x$ NSs, TB and TB/COOH-$Ti_3C_2T_x$ NSs.

effective etching of Al from Ti_3AlC_2 (Fig. S2a & b). Fig. S2 c-h depicts the elemental mapping of $Ti_3C_2T_x$ NSs which explicitly witnesses the removal of Al from the precursor and also shows the uniform distribution of all the other elements. The FESEM images of COOH-$Ti_3C_2T_x$ NSs in Fig. 2a & b further exhibits NSs-like morphology, which proves that the surface morphology remains unaltered during surface functionalization. Further, decrease in the wt% of other functional groups like -F and -Cl on COOH-$Ti_3C_2T_x$ NSs could be due to successful replacement of -COOH group on $Ti_3C_2T_x$ NSs (Fig. 2h). In addition, elemental analysis of COOH-$Ti_3C_2T_x$ NSs also confirms the absence of Al and uniform dispersion of the other elements (Fig. 2c - g).

The powder X-ray diffraction (XRD) technique was utilized to analyse the crystal structure of the $Ti_3C_2T_x$ and COOH-$Ti_3C_2T_x$ NSs and the results are depicted in Fig. 3a. XRD pattern of $Ti_3C_2T_x$ indicates the formation of characteristic peak at 6.3° corresponding to (002), and diminishing peak at 38.4° corresponding to Al confirming that $Ti_3C_2T_x$ NSs has been successfully synthesized. In the case of COOH-$Ti_3C_2T_x$ NSs, the (002) peak has shifted towards lower 2θ = 5.9°, and this could be due to the -COOH functionalization on the surface of $Ti_3C_2T_x$ NSs.[34] Further, the $Ti_3C_2T_x$ NSs and COOH-$Ti_3C_2T_x$ NSs have been investigated using thermogravimetric analysis (TGA) and the results are displayed in Fig. 3b. After subjecting the samples up to 900 °C, the obtained residual for $Ti_3C_2T_x$ and COOH-$Ti_3C_2T_x$ NSs were 82.6 wt.% and 78.1 wt.%, respectively.[35,36] The higher weight loss observed with COOH-$Ti_3C_2T_x$ NSs than that of $Ti_3C_2T_x$ NSs could be due the functionalized -COOH groups on the surface of $Ti_3C_2T_x$. Acid functionalization was further confirmed by recording Raman spectra for the synthesized $Ti_3C_2T_x$ and COOH-$Ti_3C_2T_x$ NSs as illustrated in Fig. 3c. The Raman spectra of $Ti_3C_2T_x$ NSs shows four significant peaks at 255. 2, 394.2, 629.9 and 730.9 cm^{-1} which are associated with $Ti_3C_2T_x$ NSs. These peaks correspond to in plane vibrations of Ti-C, O atoms, C atom and surface functional groups respectively.[37] Further, the peaks attributable to D and G bands (carbon atom defect peaks) were observed around 1323.8 and 1563.6 cm^{-1}.[38] After functionalization of $Ti_3C_2T_x$ NSs with -COOH groups, a slight shift in the Raman peaks along with increase in its intensity were observed with the spectrum of COOH-$Ti_3C_2T_x$ NSs and this infers that the $Ti_3C_2T_x$

View Article Online
DOI: 10.1039/D5SD00114E

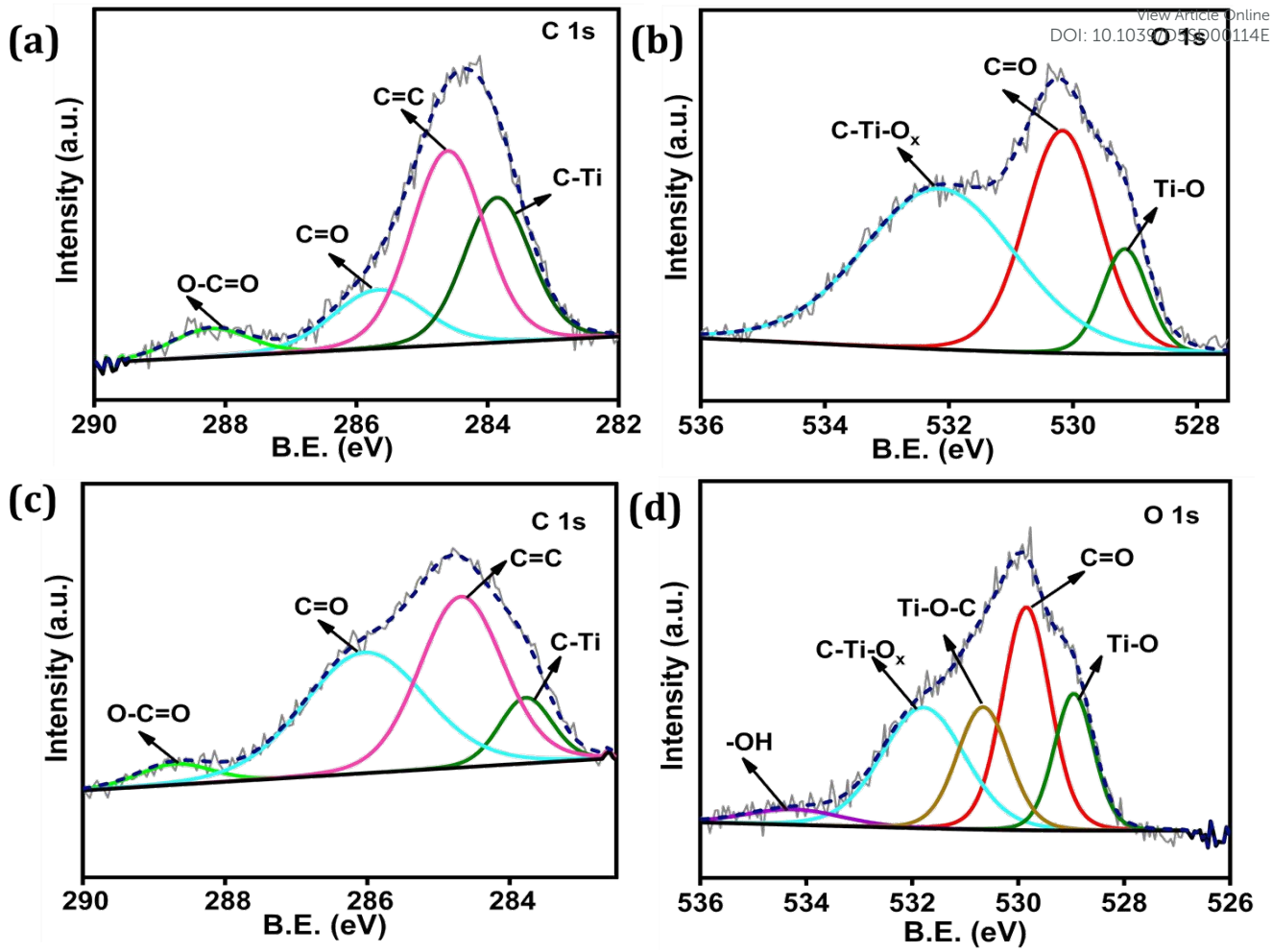

Fig. 4 C 1s and O 1s core level XPS spectra of (a, b) $Ti_3C_2T_x$ and (c, d) COOH-$Ti_3C_2T_x$ NSs.

NSs have been functionalized with –COOH groups to a greater extent.[39]

The formation of COOH-functionalized $Ti_3C_2T_x$ NSs from the OH-terminated $Ti_3C_2T_x$ NSs was investigated using FTIR spectroscopy. The FTIR spectrum (Fig. 3d) of $Ti_3C_2T_x$ NSs (blue curve) displayed the stretching and bending vibration at 3434 cm^{-1} and 1374 cm^{-1}, confirming the strong -OH terminal group on the surfaces of $Ti_3C_2T_x$ NSs. In the case of COOH-$Ti_3C_2T_x$ NSs, the peak at 1628 cm^{-1} is due to the presence of carbonyl group and the peak at 1251 cm^{-1} is the characteristic absorption peak of C-OH, confirming the presence of carboxylic group.[33] The peak at 1708 cm^{-1} could be ascribed to the ester group generated by succinic anhydride and a strong peak at 2931 cm^{-1} corresponds to the anti-symmetrical stretching vibration of C-H in COOH-$Ti_3C_2T_x$ NSs. Furthermore, after ring-opening and esterification reaction, the stretching vibration of Ti-O at 617 cm^{-1} shifted significantly to 563 cm^{-1}, which could have been influenced by the conjugated groups connected via Ti-O bonds. The covalent anchoring of TB over COOH-$Ti_3C_2T_x$ NSs through amide bond formation between the free -NH_2 in TB and -COOH of COOH-$Ti_3C_2T_x$ NSs was validated by the formation of new peaks at 3441 cm^{-1} and 1700 cm^{-1} which represent the -NH and -C=O vibrations of amide groups formed.[40]

The nature and composition of surface elements on $Ti_3C_2T_x$ NSs and COOH-$Ti_3C_2T_x$ NSs was examined through X-ray photoelectron spectroscopy (XPS) and the detailed core level spectra is illustrated in Fig. 4. The survey spectrum of $Ti_3C_2T_x$ and COOH-$Ti_3C_2T_x$ NSs in Fig. S3 shows the presence of Ti, C, O and Cl, which again evidences the effective synthesis of $Ti_3C_2T_x$ NSs by LiF/HCl etching and these results are in good agreement with the EDS results shown in Fig. 2 and Fig. S2.[41] It could be noticed from the spectra of COOH-$Ti_3C_2T_x$ NSs that the acid functionalization of $Ti_3C_2T_x$ NSs results in enhanced peak intensities for C 1s and O 1s. Fig. 4a depicts the core level spectrum of $Ti_3C_2T_x$ NSs corresponding to C 1s, wherein the peaks appearing at 283.8, 284.6, 285.6 and 288.2 eV are due to Ti-C, C=C, C=O and O-C=O, respectively.[42] It could be perceived from the C 1s spectrum (Fig. 4c), that the peaks corresponding to C=C and C=O have intensified and the peak with respect to Ti-C got diminished, which clearly indicates the increased -COOH group on COOH-$Ti_3C_2T_x$ NSs. Fig. 4b demonstrates the O1s core level spectrum of $Ti_3C_2T_x$ NSs, which further deconvoluted into three peaks and are attributed to Ti-O (529 eV), C=O (530 eV) and C-Ti-O_x (532 eV). Further, the fitted O 1s spectrum of COOH-$Ti_3C_2T_x$ NSs reveals a new peak at 530.6 eV (Fig. 4d), corresponding to the Ti-O-C covalent bond formation.[43] Fig.

View Article Online
DOI: 10.1039/D5SD00114E

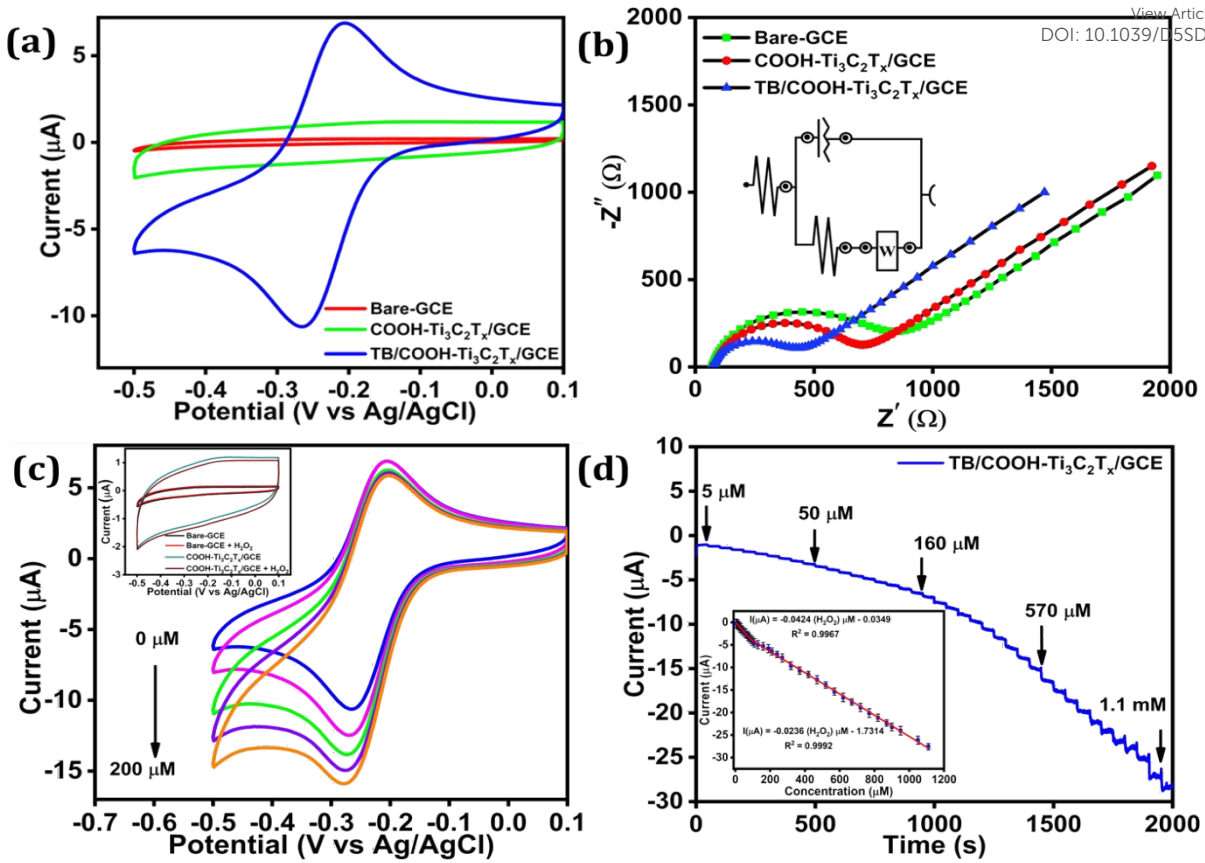

Fig. 5 (a) CV response of bare GCE (red), COOH-$Ti_3C_2T_x$/GCE (green) and TB/COOH-$Ti_3C_2T_x$/GCE (blue) in N_2 saturated 0.1 M PBS (pH 7) at a scan rate of 20 mV s^{-1} (b) Nyquist plots of the sequentially modified electrodes in 0.1 M KCl solution containing 2.5 mM $[Fe(CN)_6]^{3-/4-}$ (c) CVs of TB/COOH-$Ti_3C_2T_x$/GCE with increasing concentration of H_2O_2 (50, 100, 150 and 200 μM). Inset: CVs of bare GCE and COOH-Ti3C_2T_x/GCE in the absence and presence of 200 μM H_2O_2. (d) Amperometric (i-t) curve of TB/COOH-$Ti_3C_2T_x$/GCE towards sequential addition of H_2O_2 into constantly stirred N_2 saturated electrolyte at an applied potential of -0.25 V. Inset: Calibration plot for H_2O_2 detection.

S3 (b, c) shows the core level Ti 2p spectrum of $Ti_3C_2T_x$ NSs and COOH-$Ti_3C_2T_x$ NSs, which are deconvoluted into six peaks that are associated with Ti-C $2p_{3/2}$, Ti^{2+} $2p_{3/2}$, Ti-O $2p_{3/2}$, Ti-C $2p_{1/2}$, Ti^{2+} $2p_{1/2}$, and Ti-O $2p_{1/2}$, respectively.[44] All these detailed structural, morphological and spectral investigations explicitly confirm the successful synthesis and formation of $Ti_3C_2T_x$ NSs and COOH-$Ti_3C_2T_x$ NSs and covalent anchoring of TB on COOH-$Ti_3C_2T_x$ NSs.

3.2. Electrochemical behaviour of the TB/COOH-$Ti_3C_2T_x$ /GCE

In order to progressively investigate the electrochemical behaviour during the stepwise fabrication of the electrochemical sensor, the cyclic voltammetric (CV) response was recorded in N_2 saturated 0.1 M phosphate buffer solution (PBS) (pH 7.0) at a scan rate of 20 mV s^{-1} and the results are displayed in Fig. 5a. As expected, bare GCE and COOH-$Ti_3C_2T_x$/GCE did not show any redox peaks within the fixed potential window (0.1 to -0.5 V) of the investigation. However, the TB/COOH-$Ti_3C_2T_x$/GCE demonstrated a well-defined redox peak with a cathodic and anodic peak potentials at -0.26 V and -0.21 V with a formal potential of -0.24 V and peak separation of 50 mV, corresponding to the TB redox dye. A stable redox couple with less peak separation and prominent current response was observed only for TB/COOH-$Ti_3C_2T_x$/GCE, which could be due to firm covalent immobilization of TB and improved electrochemical active surface area and superior conductivity offered by the host $Ti_3C_2T_x$ NSs platform.

To examine the interfacial charge transfer between the electrode and electrolyte during the stepwise TB modified electrode fabrication, electrochemical impedance spectroscopy (EIS) was conducted in the solution containing 0.1 M KCl and 2.5 mM of $[Fe(CN)_6]^{4-/3-}$. The Nyquist plot presented in Fig. 5b illustrates the impedance data, which were fitted using a Randles circuit model (inset to Fig. 5b), where the diameter of the semicircle observed in the plot corresponds to the charge transfer resistance (R_{ct}). The graph corresponding to bare GCE reveals a significantly high R_{ct} value of 718 Ω, suggesting a pronounced inadequacy of electron transfer at the surface of bare GCE. Upon the integration of COOH-$Ti_3C_2T_x$ NSs over GCE, the R_{ct} notably dropped to 592 Ω, emphasizing the improved conductivity imparted by COOH-$Ti_3C_2T_x$ NSs. Subsequent modification with TB in TB/COOH-$Ti_3C_2T_x$/GCE resulted in a remarkably low R_{ct} of 340 Ω, highlighting the superior electron transfer efficiency facilitated by the mediator. According to the EIS results, the facile COOH-$Ti_3C_2T_x$ NSs platform offers good

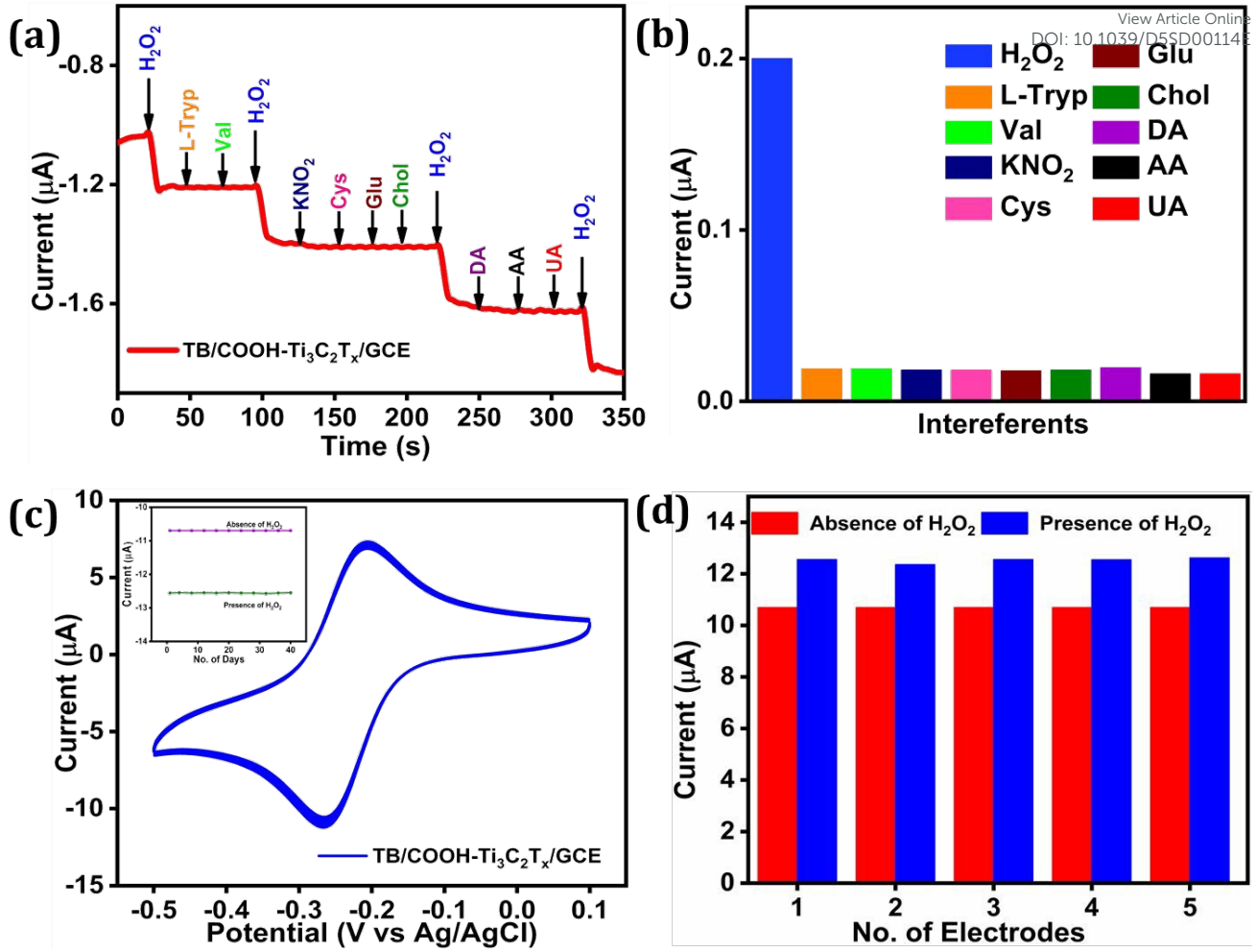

Fig. 6 (a) Effect of interference towards H_2O_2 determination (5 μM) in the presence of other interferents (0.5 mM) in N_2 saturated 0.1 M PBS (pH 7) (b) corresponding bar diagram. (c) CV curve of TB/COOH-$Ti_3C_2T_x$/GCE for 50 continuous cycles. Inset: plot of day-to-day current response of the fabricated sensor in the presence (green) and absence (pink) of 50 μM H_2O_2. (d) Bar diagram relating the current response with and without H_2O_2 (50 μM) for five identically fabricated sensors.

conductivity, which makes it appropriate for electrochemical sensing. In order to examine the nature of electrochemical process occurring at the fabricated electrochemical sensor TB/COOH-$Ti_3C_2T_x$/GCE, the scan rate effect was performed in 0.1 M PBS by varying the scan rate from 10 mV s^{-1} to 100 mV s^{-1} (Fig. S4a). Cathodic and anodic peak currents enhanced incrementally with respect to scan rate and the plot of current versus square root of scan rate exhibited linearity, indicating the diffusion controlled redox process occurring at the TB modified electrode (Fig. S4b). and

3.3. Electrocatalytic activity of the TB/COOH-$Ti_3C_2T_x$/GCE towards H_2O_2 reduction

Improved electrochemical behaviour with well-defined redox peak of the TB/COOH-$Ti_3C_2T_x$/GCE inspired us to probe its catalytic efficiency towards the electrocatalytic detection of H_2O_2. Therefore, electrocatalytic activity of bare GCE, COOH-$Ti_3C_2T_x$/GCE and TB/COOH-$Ti_3C_2T_x$/GCE towards H_2O_2 sensing was examined by recording CV in the presence and absence of H_2O_2 in N_2 saturated PBS (0.1 M, 7 pH). The bare (red curve) and COOH-$Ti_3C_2T_x$/GCE (brown curve) did not exhibit any electrocatalytic response upon addition of H_2O_2 (inset Fig. 5c) whereas, TB/COOH-$Ti_3C_2T_x$/GCE demonstrated an excellent catalytic response with increasing cathodic peak current. Fig. 5c depicts the CV response of TB/COOH-$Ti_3C_2T_x$/GCE towards raising concentrations of 0, 50, 100, 150 and 200 μM of H_2O_2 at a scan rate of 20 mV s^{-1}. For every successive addition of H_2O_2, the cathodic peak current exhibits a linear increase at -0.25 V, while the anodic peak current displays a slight decline. This response signifies the TB mediated electrocatalytic reduction of H_2O_2 occurring at the TB/COOH-$Ti_3C_2T_x$/GCE electrochemical sensor. During the electrocatalytic process, TB gets reduced when its reduction potential is attained. The reduced TB further reacts with H_2O_2 at the electrode-electrolyte interface and subsequently the TB mediator gets oxidized. These reactions (Eqs 1and 2) repeat in a cycle as far as the analyte, H_2O_2 is available at the surface of TB/COOH-$Ti_3C_2T_x$/GCE, which results in a stable enhancement of the cathodic current with every addition of H_2O_2.[19,45] These results confirm that COOH-$Ti_3C_2T_x$ acts as a versatile host platform for immobilizing TB, which caused remarkable electrocatalytic activity during the reduction of H_2O_2. Thus, the electrocatalytic efficacy of the TB/COOH-$Ti_3C_2T_x$/GCE sensor is attributed to the enhanced

View Article Online
DOI: 10.1039/D5SD00114E

Table 1. Performances of TB/COOH-$Ti_3C_2T_x$/GCE sensor towards H_2O_2 detection compared with recently reported non-enzymatic electrochemical sensors.

Electrode material	Analyte	Operating potential (V)	Linear range (μM)	LOD (μM)	Sensitivity	Ref.
$ZnFe_2O_4$/g-C_3N_4	H_2O_2	1	5 – 200	1	189.5 μA mM^{-1} cm^{-2}	2
MX/CS/PB/GCE	H_2O_2	0	0.05 – 667	0.004	-	46
CC/Nb_2CT_x@PB480	H_2O_2	-0.1	1 – 100	20	-	47
Co_3O_4/ATNTs	H_2O_2	-0.6	1.27 - 26.80	6.71	39.53 μA mM^{-1} cm^{-2}	48
Gr/P-CoHCF-NSPs	H_2O_2	0.95	1 - 1000	1	914 μA mM^{-1} cm^{-2}	49
MWCNT-$Ti_3C_2T_x$-Pd	H_2O_2	0	50 - 18000	3.83	293.85 μA mM^{-1} cm^{-2}	50
Cu/CoO NCs	H_2O_2	-0.2	100 - 1000	1.85	27.7 μA mM^{-1} cm^{-2}	51
Co_3O_4 nPTLS	H_2O_2	-1.2	25 - 5000	5.2	201 μA mM^{-1} cm^{-2}	52
Mn_xO_y/$Ti_3C_2T_x$-GCE	H_2O_2	0.89	0.05 - 650	0.0045	17,420 μA mM^{-1} cm^{-2}	53
Pd-Ti_2NT_xMXene/GCE	H_2O_2	0.4	5 - 200	0.72	0.825 μA μM^{-1} cm^{-2}	54
CuO-CeO_2/MXene	H_2O_2	0.3	5 - 100	1.7	-	55
TB/COOH-$Ti_3C_2T_x$/GCE	**H_2O_2**	**-0.25**	**5 – 100 & 100 - 1100**	**1.5**	**0.61 μA μM^{-1} cm^{-2}**	**This work**

conductivity and active sites afforded by MXene and the improved electrical wiring between TB mediator and MXene platform through covalent immobilization of TB. Electrochemical detection of H_2O_2 at TB/COOH-$Ti_3C_2T_x$/GCE is represented as follows:

$$TB(Oxd) + 2e^- + 2H^+ \rightarrow TB(Red) \quad (1)$$

$$TB(Red) + H_2O_2 \rightarrow TB(Oxd) + H_2O \quad (2)$$

3.4. Amperometric determination of H_2O_2 at TB/COOH-$Ti_3C_2T_x$/GCE

TB/COOH-$Ti_3C_2T_x$/GCE demonstrated excellent electrocatalytic response towards H_2O_2 detection in CV investigations, which prompted us to authenticate the determination of H_2O_2 in dynamic conditions using amperometric measurements. The maximum catalytic response of the TB/COOH-$Ti_3C_2T_x$/GCE for H_2O_2 reduction was observed at -0.25 V, which was fixed as the applied potential to perform amperometric studies. Fig. 5d demonstrates the stepwise amperometric response of the TB/COOH-$Ti_3C_2T_x$/GCE at an applied potential of -0.25 V for consecutive addition of H_2O_2 into a stirred (300 rpm) N_2 saturated PBS (0.1 M, pH 7.0) electrolyte. For every successive insertion of H_2O_2 at TB/COOH-$Ti_3C_2T_x$/GCE, an instantaneous rise in catalytic current was observed and reached its steady state current within <3 s. The corresponding calibration plot of the amperometric response was obtained by plotting the H_2O_2 concentration against the increase in current response achieved at TB/COOH-$Ti_3C_2T_x$/GCE (inset Fig. 5d). The fabricated sensor TB/COOH-$Ti_3C_2T_x$/GCE exhibited excellent catalytic response towards H_2O_2 reduction in two concentration ranges from 5 μM to 100 μM and 100 μM to 1.1 mM after which the linearity of the calibration plot deflects gradually. Further, the LOD and sensitivities of the constructed sensor were estimated to be 1.5 μM and 0.61 μA μM^{-1} cm^{-2} and 0.33 μA μM^{-1} cm^{-2}, respectively. The obtained results are comparable or better than the recently reported nonenzymatic electrochemical sensor for H_2O_2 reduction as illustrated in Table 1. The better sensitivity and enhanced catalytic activity of the TB/COOH-$Ti_3C_2T_x$/GCE is ascribed to the fast electron transfer ability of the TB mediator and high conductivity offered by $Ti_3C_2T_x$ NSs host platform.

3.5. Interference, Stability and reproducibility studies of TB/COOH-$Ti_3C_2T_x$/GCE

The selectivity of the modified sensor towards H_2O_2 is a crucial aspect for real time analysis and it was assessed in the presence of other

concomitant interfering analytes including ascorbic acid (AA), dopamine hydrochloride (DA), Uric acid (UA), glucose (Glu), cholesterol (Chol), tryptophan (L-Tryp), cystine (Cys), Valine (Val) and potassium nitrite (KNO_2). As it could be observed in Fig. 6a, only H_2O_2 injection exhibited a notable current response, and even ten times larger concentrations of other species did not significantly change the current response (Fig. 6b). A rapid response attained during the addition of H_2O_2 is due to the enhanced electrical communication between the TB and COOH-$Ti_3C_2T_x$ NSs during the covalent immobilization. Further, the selectivity of the sensor could be ascribed to the selective electrocatalytic reduction of H_2O_2 by the TB mediator at the chosen lower working potential of -0.25 V. In addition, the stability of the constructed TB/COOH-$Ti_3C_2T_x$/GCE was examined by reanalysing the stored electrochemical sensor and performing continuous potential cycling. Fifty successive cyclic voltammograms were recorded with TB/COOH-$Ti_3C_2T_x$/GCE and the observations are displayed in Fig. 6c. The results exhibited outstanding cycling stability with no discernible change in peak potentials and peak currents. Fig. 6c inset displays the current response recorded at regular intervals over a 40-day storage period of the developed electrochemical sensor with and without H_2O_2. During this time, the sensor TB/COOH-$Ti_3C_2T_x$/GCE retained its initial response of 96.4% and 93.6% in the absence and presence of H_2O_2, respectively. The sensor achieved this robust cyclic as well as long term stability as an outcome of the stable immobilization strategy adapted for the water-soluble mediator TB on COOH-$Ti_3C_2T_x$. Though the $Ti_3C_2T_x$ MXenes afford excellent electrochemical properties, they tend to oxidize upon long term exposure to ambient conditions or upon subjecting to higher positive potentials. Thus, these sensors have to be operated at negative or lesser positive potentials and have to be stored in inert conditions when not in use. Efforts to improve the stability of these MXenes through structural modulation via judicious interfacial engineering and also designing new MXenes with enhanced stability are underway in our laboratory. Reproducibility of the sensor was examined by fabricating various TB modified electrodes with identical procedure and recording their current response in the presence and absence of H_2O_2 (Fig. 6d). The results demonstrated that the fabricated batch of TB sensors revealed very good reproducibility with no noticeable decline in current response. The better storage and cyclic stability of the proposed electrochemical sensor could again be credited to the effective covalent immobilization of TB over the highly conductive substrate of COOH-$Ti_3C_2T_x$.

3.6. Real time detection of H_2O_2

In order to investigate the efficacy and suitability of TB/COOH-$Ti_3C_2T_x$/GCE in real-time biological samples, H_2O_2 determination was performed by spiking the known concentration of H_2O_2 in real samples, such as diluted milk and goat serum (purchased from the local slaughter house), and the obtained results are displayed in Table 2. In brief, milk and serum (1 mg/mL) samples were diluted using 0.1 M PBS and then the known concentrations of H_2O_2 was spiked by standard addition method (Fig. S5). Also, we have compared our results with the standard permanganate titration for H_2O_2 determination. The estimated concentrations of H_2O_2 in milk and serum samples using the constructed electrochemical sensor matched very well with the added amount and also with the standard titration method. The recovery values achieved using the constructed electrochemical sensor were between 97.8% and 102.0% with lower RSD values. These findings demonstrate that TB/COOH-$Ti_3C_2T_x$/GCE could effectively detect H_2O_2 in real biological samples.

Table 2. Determination of H_2O_2 in real samples.

Sample	Spiked (μM)	Found (μM)		Recovery ± RSD (%)
		Standard method	Our method[a]	
Milk	50	49.8	49.2	98.4 ± 1.24
	150	150.1	152.3	101.5 ± 1.02
Goat serum	50	49.9	48.9	97.8 ± 1.13
	150	151.2	153.1	102.0 ± 1.1

[a]Measurements were performed in triplicate

4. Conclusion

This report presents the design and development of an efficient electrochemical sensor for the sensitive and specific detection of H_2O_2. The -NH_2 groups in TB were chemically bonded to the -COOH groups in COOH-$Ti_3C_2T_x$ NSs using EDC/NHS cross-coupling chemistry. The large surface area of COOH-$Ti_3C_2T_x$ NSs not only provided a good electron tunnelling path for enhanced conductivity and sensitivity, but it also served as a versatile host to offer an increased loading of the redox mediator. The mediator TB exhibited well defined redox behaviour with high stability and good reproducibility due to the stable covalent immobilization over COOH-$Ti_3C_2T_x$ NSs. Further, the fabricated electrochemical sensor based on TB/COOH-$Ti_3C_2T_x$/GCE demonstrated excellent catalytic response for H_2O_2 detection at a low operating potential of -0.25 V with high selectivity. The analytical properties like wide concentration range, low LOD, competent sensitivity and interference-free sensing of TB/COOH-$Ti_3C_2T_x$/GCE reveals the great potential of the TB sensor towards the early diagnosis of various diseases through the detection of H_2O_2 biomarker. Prudent surface engineering of $Ti_3C_2T_x$ NSs towards development of a nonenzymatic electrochemical sensor established in this work could open new path for designing broad range of devices in healthcare diagnostics.

Data availability

The data supporting this article have been included as part of the ESI. The original files will be made available on request.

Author contributions

Devarasu Mohanapriya: Conceptualization, methodology, investigation, validation, writing – original draft. Kathavarayan Thenmozhi: Conceptualization, resources, supervision, project administration, writing – review & editing.

Conflicts of interest

There are no conflicts to declare.

Acknowledgements

This work was financially supported by Vellore Institute of Technology (VIT) Vellore under the Faculty Seed Grant (RGEMS) (Sanction Order No.: SG20220001). The authors also acknowledge the Central Research Facilities (CRF), Vellore Institute of Technology (VIT) for providing instrumentation facilities.

References

1 R. Banavath, R. Srivastava and P. Bhargava, *ACS Appl. Nano Mater.*, 2021, **4**, 5564–5576.

2 M. Ye, C. Yang, Y. Sun, J. Wang, D. Wang, Y. Zhao, Z. Zhu, P. Liu, J. Zhu, C. Li, W. Peng, N. Zhang and Y. Dong, *ACS Appl. Nano Mater.*, 2022, **5**, 10922–10932.

3 X. Chai, S. Ye, F. Wang, H. Yuan, M. Liu, F. Fan, L. Zhang, X. Zhang, T. Wang and Y. Fu, *Inorg. Chem.*, 2023, **62**, 10694–10703.

4 Z. Yang, Z. Tian and C. Qi, *ACS Appl. Nano Mater.*, 2023, **6**, 21141–21151.

5 J. E. Giaretta, H. Duan, F. Oveissi, S. Farajikhah, F. Dehghani and S. Naficy, *ACS Appl. Mater. Interfaces*, 2022, **14**, 20491–20505.

6 W. Chen, S. Cai, Q. Q. Ren, W. Wen and Y. Di Zhao, *Analyst*, 2012, **137**, 49–58.

7 V. P. Sruthi, S. Sarfudeen, T. Panda, K. Thenmozhi and S. Senthilkumar, *J. Mater. Chem. A*, 2025, **13**, 8343.

8 V. P. Sruthi and S. Senthilkumar, *J. Mater. Chem. C*, 2024, **12**, 8924–8934.

9 D. Mohanapriya and K. Thenmozhi, *J. Mater. Chem. B*, 2025, **13**, 2306 .

10 A. Sugunan, A. V. Rethnakumaran and M. M. Menamparambath, *Sensors and Diagnostics*, 2024, **3**, 1769–1788.

11 J. Liu, M. Li, W. Liu, Z. Hao, F. Zhang, H. Pang, R. Zhang and L. Zhang, *J. Electroanal. Chem.*, 2024, **954**, 118060.

12 B. Luo, X. Li, J. Yang, X. Li, L. Xue, X. Li, J. Gu, M. Wang and L. Jiang, *Anal. Methods*, 2014, **6**, 1114–1120.

13 J. Guo, S. Li, J. Wang and J. Wang, *Biosens. Bioelectron.*, 2022, **198**, 113820.

14 S. Liu, B. Yu, T. Fei and T. Zhang, *Sensors Actuators, B Chem.*, 2014, **201**, 240–245.

15 C. Bruckschlegel, V. Fleischmann, N. Gajovic-Eichelmann and N. Wongkaew, *Talanta*, 2025, **291**, 127850.

16 H. Wu, W. Zheng, Y. Jiang, J. Xu and F. Qiu, *New J. Chem.*, 2021, **45**, 21676–21683.

17 A. Emin, A. Ding, S. Ali, M. Chhattal, S. Ali, A. Parkash and Q. Li, *Microchem. J.*, 2024, **207**, 111972.

18 R. Peng, A. Offenhäusser, Y. Ermolenko and Y. Mourzina, *Sensors Actuators, B Chem.*, 2020, **321**, 128437.

19 K. Thenmozhi and S. Sriman Narayanan, *Anal. Bioanal. Chem.*, 2007, **387**, 1075–1082.

20 E. Martínez-Periñán, A. Domínguez-Saldaña, A. M. Villa-Manso, C. Gutiérrez-Sánchez, M. Revenga-Parra, E. Mateo-Martí, F. Pariente and E. Lorenzo, *Sensors Actuators B Chem.*, 2023, **374**, 132761.

21 A. Esokkiya, S. Sudalaimani, K. Sanjeev Kumar, P. Sampathkumar, C. Suresh and K. Giribabu, *ACS Omega*, 2021, **6**, 9528–9536.

22 D. Manoj, K. Theyagarajan, D. Saravanakumar, S. Senthilkumar and K. Thenmozhi, *Biosens. Bioelectron.*, 2018, **103**, 104–112.

23 M. Zhang and W. Gorski, *J. Am. Chem. Soc.*, 2005, **127**, 2058–2059.

24 Y. M. Liu, C. Punckt, M. A. Pope, A. Gelperin and I. A. Aksay, *ACS Appl. Mater. Interfaces*, 2013, **5**, 12624–12630.

25 X. Liang, Y. Zhou, J. M. S. Almeida and C. M. A. Brett, *J. Electroanal. Chem.*, 2023, **936**, 117366.

26 H. Wang, Q. Dong, L. Lei, S. Ji, P. Kannan, P. Subramanian and A. P. Yadav, *Nanomaterials*, 2021, **11**, 20857.

27 P. Kanagavalli, C. Andrew, M. Veerapandian and M. Jayakumar, *TrAC - Trends Anal. Chem.*, 2021, **143**, 116413.

28 K. Sakthivel, S. Balasubramanian, G. P. Chang-Chien, S. F. Wang, Ahammad, W. Billey, J. Platero, T. Soundappan and P. Sekhar, *ECS Sens. Plus.*, 2024, **3**, 020605.

29 S. Ullah, T. Najam, A. ur Rehman, S. S. Alarfaji, M. A. Ahmad, S. Riaz, B. Akkinepally, S. S. A. Shah and M. A. Nazir, *J. Alloys Compd.*, 2024, **1001**, 175172.

30 D. Mohanapriya, J. Satija, S. Senthilkumar, V. Kumar Ponnusamy and K. Thenmozhi, *Coord. Chem. Rev.*, 2024, **507**, 215746.

31 A. Vahidmohammadi, J. Moncada, H. Chen, E. Kayali, J. Orangi, C. A. Carrero and M. Beidaghi, *J. Mater. Chem. A*, 2018, **6**, 22123–22133.

32 S. B. Ambade, L. A. Kesner, M. K. Abdel-Rahman, D. H. Fairbrother and Z. Rosenzweig, *ACS Appl. Nano Mater.*, 2023, **6**, 4898–4909.

33 X. Liu, Y. Qiu, D. Jiang, F. Li, Y. Gan, Y. Zhu, Y. Pan, H. Wan and P. Wang, *Microsystems Nanoeng.*, 2022, **8**, 35, .

34 M. Alhabeb, K. Maleski, B. Anasori, P. Lelyukh, L. Clark, S. Sin and Y. Gogotsi, *Chem. Mater.*, 2017, **29**, 7633–7644.

35 A. P. Isfahani, A. A. Shamsabadi, F. Alimohammadi and M. Soroush, *J. Hazard. Mater.*, 2022, **434**, 128780.

36 S. Shah, I. Mubeen, E. Pervaiz and H. Nasir, *FlatChem*, 2023, **41**, 100544.

37 P. Najmi, N. Keshmiri, M. Ramezanzadeh, B. Ramezanzadeh and M. Arjmand, *Chem. Eng. J.*, 2023, **456**, 141001.

38 K. Wang, L. Shen, Q. Zhu, R. Bo, R. Lu, X. Lu and Z. Fu, *Chem. Eng. J.*, 2023, **452**, 139156.

39 I. M. Chirica, A. G. Mirea, T. Şuteu, A. Kuncser, Ş. Neaţu, M. Florea, M. W. Barsoum and F. Neaţu, *ACS Sustain. Chem. Eng.*, 2024, **12**, 9766–9776.

40 B. Scheibe, K. Tadyszak, M. Jarek, N. Michalak, M. Kempiński, M. Lewandowski, B. Peplińska and K. Chybczyńska, *Appl. Surf.*

View Article Online
DOI: 10.1039/D5SD00114E

Sci., 2019, **479**, 216–224.

41 C. Roy, S. K. De, P. Banerjee, S. Pradhan and S. Bhattacharyya, *J. Alloys Compd.*, 2023, **938**, 168471.

42 L. He, L. Wang, L. Yang, J. Cui, X. Jiang, Y. Ge, J. Zhang, J. Yang, Q. Hou and J. Shen, *ACS Appl. Nano Mater.*, 2024, **7**, 14769–14779.

43 B. S. Shen, H. Wang, L. J. Wu, R. S. Guo, Q. Huang and X. Bin Yan, *Chinese Chem. Lett.*, 2016, **27**, 1586–1591.

44 A. Pazniak, P. Bazhin, N. Shplis, E. Kolesnikov, I. Shchetinin, A. Komissarov, J. Polcak, A. Stolin and D. Kuznetsov, *Mater. Des.*, 2019, **183**, 108143.

45 P. Yaiwong, K. Iamsawat, S. Wiratchan, W. Jumpathong, N. Semakul, S. Bamrungsap, J. Jakmunee and K. Ounnunkad, *Food Chem.*, 2024, **439**, 138147.

46 F. Zhu, X. Wang, X. Yang, C. Zhao, Y. Zhang, S. Qu, S. Wu and W. Ji, *Anal. Methods*, 2021, **13**, 2512–2518.

47 A. Mohan Arjun, N. Shabana, M. Ankitha and P. Abdul Rasheed, *Microchem. J.*, 2023, **185**, 108301.

48 R. Ullah, M. A. Rasheed, S. Abbas, K. ul Rehman, A. Shah, K. Ullah, Y. Khan, M. Bibi, M. Ahmad and G. Ali, *Curr. Appl. Phys.*, 2022, **38**, 40–48.

49 R. Banavath, R. Srivastava and P. Bhargava, *Catal. Sci. Technol.*, 2022, **12**, 2369–2383.

50 J. Zhang, M. Lu, H. Zhou, X. Du and X. Du, *Int. J. Mol. Sci.*, 2022, **23**, 0–13.

51 C. Liu, J. Choi, J. Hyun, S. H. Bhang and T. Yu, *Korean J. Chem. Eng.*, 2023, **40**, 2771–2777.

52 V. Gerbreders, M. Krasovska, E. Sledevskis, I. Mihailova and V. Mizers, *Micromachines*, 2024, **15**, 311.

53 B. Wanga, S. M. Khoshfetrat and H. Mohamadimanesh, *Microchem. J.*, 2024, **207**, 111796.

54 Y.Zhang, L. He, X. Sun, C. Yang and J. Li, *chemistryselect*, 2024, **9**, 44.

55 K. Zhou, Y. Li, S. Zhuang, J. Ren, F. Tang, J. Mu and P. Wang, *J. Electroanal. Chem.*, 2022, **921**, 116655.

Data availability statement

View Article Online
DOI: 10.1039/D5SD00114E

The data supporting this article have been included as part of the Electronic Supplementary Information. The original files will be made available on request.